ANALYSIS OF HIGH FLIGHT SPEEDS ON COMPOUND ROTORCRAFT DESIGN

Peter Weiand, German Aerospace Center (DLR), Braunschweig, Germany
Kagan Atci, German Aerospace Center (DLR), Braunschweig, Germany
Dominik Schwinn, German Aerospace Center (DLR), Stuttgart, Germany

Abstract

Capabilities for new medium-sized utility rotorcraft with enhanced flight speeds have been investigated in recent years by numerous research studies. An opportunity for realization of such a configuration may come with the NATO project NGRC, which is considering a desired flight speed of up to 220 kn and not less than 180 kn. DLR supported these investigations with a high-speed rotorcraft design study. The objective was an increase of flight speed by 50% to about 240 kn, which resulted in tremendous amount of required power. The configuration was considered to be very performant, but inefficient with respect to the conventional flight envelope. In this paper, the required speed interval for project NGRC is investigated. The design space is defined by four design speeds besides of three required flight distances. The baseline configuration is a revised high-speed rotorcraft from the first study, featuring a new main rotor. The twelve design configurations are analyzed considering their characteristics like installed power and flight performance. The increase in size and weight is continuous with increasing speed and range. Recommendations for the further progress are defined based on the results of the design study.

NOTATION

AVT	Applied Vehicle Technology
BEM	Basic Empty Mass
CPACS	Common Parametric Aircraft Configuration Schema
DLR	German Aerospace Center (DLR)
HOGE	Hover out of ground effect
HOST	Helicopter Overall Simulation Tool
HSR	High-Speed Rotorcraft
MCP	Maximum Continuous Power
MTOM	Maximum Take-Off Mass
NATO	North Atlantic Treaty Organization
NATO-GR	NATO Generic Rotorcraft
NGRC	Next Generation Rotorcraft Capabilities
C_d	Drag coefficient
C_T	Thrust coefficient
DL	Disc loading, N/m²
Ma	Mach number
N	Number of blades
P	Power, W
R	Rotor radius, m
a	Speed of sound, m/s
c	Mean blade chord, m
g	Gravitational acceleration, 9.81 m/s²
m	Mass, kg
r	Nondimensional rotor radius
v_h	Horizontal flight speed, m/s
Θ	Main rotor control values, deg
Θ_{twist}	Blade twist, deg
Ψ	Rotor azimuth, deg
α	Angle of attack, deg
η	Control surface deflection, deg
η_{mech}	Mechanical efficiency
μ	Advance ratio
ρ	Density of air, kg/m³
σ	rotor solidity

1. INTRODUCTION

1.1. Background

The development of a new medium multirole helicopter for the European NATO nations has progressed in the recent years. Current estimations point out that European NATO countries are facing a retirement and consequently replacement of most of their medium rotorcraft fleet in the period from 2030 to 2055. An estimated demand by the NATO nations (not including the US) suggests the procurement of no less than 900 medium-size multirole rotorcraft. This number explicitly excludes the corresponding rotorcraft fleet of the US armed forces. Project Next Generation Rotorcraft Capability (NGRC) conceptualizes a medium rotorcraft platform with a desired initial operating capability around 2040. Currently, the project NGRC is processing the concept stage until end of 2025, led by the NATO Support and Procurement Agency (NSPA). Within the project, the requirements for a new medium utility transport rotorcraft were established.

The German Aerospace Center (DLR) developed capabilities for the integrated design of rotorcraft. The focus of current investigations includes conventional helicopters, multi-rotor configurations for lower flight speeds, as well as high-speed compound rotorcraft. The use cases are tailored to helicopters in emergency medical services [1] and defense technology [2]. With these expertise DLR supports NGRC via contributing to several NATO AVT groups and the continuous consulting of the Army Concepts and Capabilities Development Centre of the German Armed Forces.

1.2. Preceding Design Study

The scientific question for the initial design study was the influence of an increased maximum speed by about 50% on the rotorcraft [2]. This investigation into high-speed configurations coincided with several studies over the last 15 years, dealing with the extension of the rotor flight envelope. Significant examples include the sizing of a compound rotorcraft with NDARC (Design and Analysis of Rotorcraft) as early as 2010 [3] and the recent flight tests of the AIRBUS RACER presented in 2025 [4].

In the previous study, a representative medium-size utility rotorcraft with a maximum take-off mass (MTOM) of about 10 t was modeled and analyzed as a reference. The reference configuration followed the concept of a NATO Generic Rotorcraft (NATO-GR), based on the public available data of a UH-60 Blackhawk [5, 6]. Based on this reference, a high-speed rotorcraft (HSR) was sized to meet the same mission requirements, except for the increase in maximum design speed from 160 kn to 240 kn (82 m/s to 125 m/s) for the HSR.

The design environment Integrated Rotorcraft Initial Sizing (IRIS) served as the primary tool box for all tasks in this study. The HSR was then modeled and sized using IRIS. Subsequently, the HSR was analyzed in comparison with the NATO-GR. Figure 1 shows the NATO-GR (above) and HSR (below) from the preceding study.

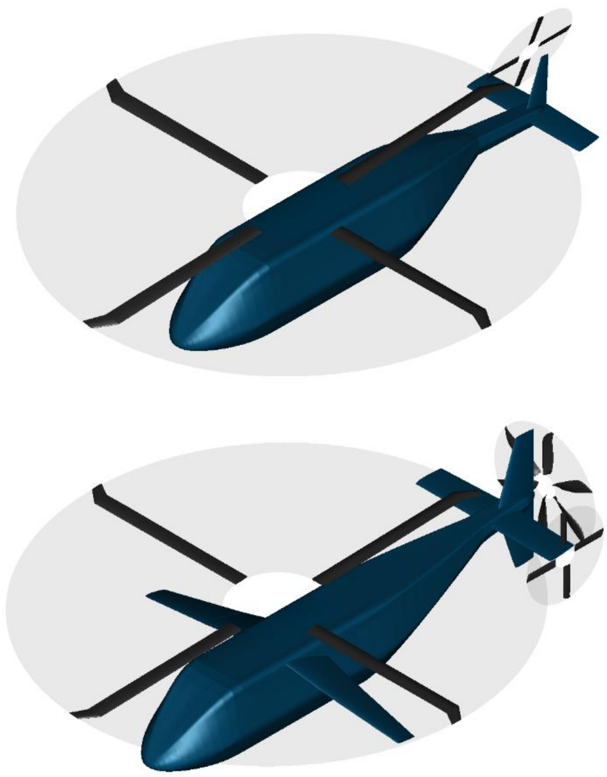

Figure 1: 3D models of the NATO generic rotorcraft (above) as reference configuration and the high-speed rotorcraft (below) as design configuration.

The results of the study pointed out the substantial increase of the maximum take-off mass (MTOM), exceeding 15 t. The very high amount of installed power resulted in a shift of the best points of operation to higher flight speeds. This led to a diminishing of efficiency in the conventional flight envelop up to 82 m/s. In conclusion, the study highlighted, that flight speeds of 125 m/s are achievable by enhanced and highly unconventional configurations, but not reasonable for a tactical medium rotorcraft designed for the European theater. The design configuration showed to be very effective but less efficient.

1.3. Motivation

The desired flight speed in project NGRC is 113 m/s (220 kn), but with a lower threshold of not less than 93 m/s (180 kn). With the 2024 HSR study [2], a possible speed range up to 125 m/s (243 kn) and above was investigated. The reference configuration in this context had a design speed of 82 m/s (160 kn), which is considered insufficient. On the other hand, the high-speed of 125 m/s resulted in an effective but inefficient rotorcraft.

In this work, the design and sizing of the HSR configuration are revised based on the lessons learned from the previous study and the adapted design requirements. The goal is an investigation with respect to maximum flight speed and mission range. It is of particular importance to show the differences between the results of such design configurations for varying requirements.

The paper begins with the overview of the design synthesis of the HSR. The next step is a revision of the HSR configuration, in particular its main rotor. This is followed by the definition of the design requirements for this study. The discussion of results is conducted and the paper is concluded with summary and outlook.

2. DESIGN SYNTHESIS OF THE HIGH-SPEED CONFIGURATON

2.1. Design Framework

The DLR's rotorcraft design environment IRIS is a modular framework with an open design space for different configurations. Current design studies cover standard configurations with a main rotor and anti-torque device, rpm-controlled multirotor configurations and high-speed compound configurations. The framework itself consists of several tools from individual disciplines. These tools are arranged in different workflows for tasks such as model initialization, mission evaluation and sizing. IRIS applies the same collaboration doctrine for rotary-wing design, that was originally developed for fixed-wing design at DLR. Here, the data model CPACS (Common Parametric Aircraft Configuration Schema) [7–9] enables a universal interface between the tools. Remote Component Environment (RCE) [10] is a collaboration software developed by DLR. RCE enables the integration of tools located on different servers into one framework, as well as the buildup of the workflows.

One progressive approach for such an environment was the integration of the comprehensive flight mechanics code Helicopter Overall Simulation Tool (HOST) [11], developed by Airbus Helicopters. HOST is used for all trim and performance calculations in the design and analysis workflows. The advantage of this tool integration is the use of a single flight model from the conceptual design up to piloted flight simulation. Hence, the focus is on the fidelity of the flight model and not the implementation of the simulation. The structure of the solver allows an open approach for various configurations. Particular important is the universal generation of the flight model from the CPACS data model by a rule-based generator and the full control of the computation from the process without the user being in direct control of HOST. This also includes a variable setup of the trim rules. Pre-work has started to integrate the DLR-developed comprehensive code MAECOsim© [12] into IRIS.

2.2. Compound Rotorcraft

The extension of the flight envelope for a rotary-wing aircraft is a configuration decision. When going beyond the speed limits of conventional helicopters, three reliable configuration types can be considered: a convertible or tilt rotor configuration, a coaxial lift-offset configuration, and a conventional single main rotor supported by a wing. The latter two are both supported by propulsive elements, typically propellers. In the first study, a conventional medium-size helicopter was modified to a compound rotorcraft with the intention of increasing the flight speed by about 50%. Hence, a single main rotor – tail rotor configuration with wing and propeller was chosen.

For a single main rotor, which delivers vertical and horizontal thrust, aerodynamics will limit the flight speed by blade stall. On the advancing side, high Mach numbers result in transonic drag rise and on the retreating side and high angles of attack result in blade stall. The drag of the fuselage increases with flight speed, requiring the rotor to deliver more propulsive force, resulting in fuselage pitch angles of larger magnitude, which increases the drag even more.

The first measure is to decouple propulsive and vertical thrust by adding for instance a propeller that delivers sufficient thrust to counteract the high drag at advanced flight speeds, as 50% increase in speed will result in 125% more drag on the fuselage.

The second measure is to slow down the main rotor by keeping the tip Mach number on the advancing side constant to a maximum allowable critical value. The decrease in rotational speed will result in a reduction of the rotor thrust. Equation (1) shows the relation between the advance ratio μ, the critical Mach number Ma_{crit}, the speed of sound a and the horizontal velocity v_h, considering the angle of the tip path plan to be zero and neglectable.

(1) $$\mu = \frac{v_h}{Ma_{crit}\, a - v_h}$$

The large area of reversal flow on the rotor plane implies a loss in lift, which must be balanced with the advancing side. To counteract this strong asymmetrical condition, the rotor thrust must be limited to avoid a pitch-up moment. A sensible value for the reduction of the blade loading, at an advance ratio around $\mu \approx 0.7$, is found with $(C_T/\sigma)_{red} = 0.05$. The blade loading of the NATO-GR in hover out of ground effect (HOGE) with rotational speed at 100% is $C_T/\sigma = 0.0939$. With equation (2), the reduction of the main rotor thrust can be evaluated, depending on air density ρ, number of blades N, mean chord c, rotor radius R, tip speed and the reduced blade loading $(C_T/\sigma)_{red}$.

(2) $$T = \left(\frac{C_T}{\sigma}\right) \rho \left(Ma_{crit}\, a\, v_h\right)^2 N\, c\, R$$

Apparently, the rotor thrust will be decreased by the limitation of the Mach number on the advancing side. Furthermore, by limiting the blade loading, the rotor thrust is reduced even further. Due to the reduced thrust and inflow, the twist of the blade must be reduced to avoid stall on the outer blade at $\Psi = 90°$.

As a third measure, to allow the reduction of the main rotor thrust, a wing has to be integrated to compensate for the residual lift. To ensure the controllability in the extended flight envelope, the wings, the horizontal and the vertical stabilizer must be equipped with control surfaces.

The decision was made for a compound rotorcraft featuring one main rotor, one tail rotor, one propeller, a wing, and an empennage. Several reasons led to the selection of this rotor configuration. Most important is the avoidance of propellers on the sides of the fuselage. This is mandatory for the integration of the vehicle into a tactical environment. In contrast to two counter-rotating propellers, a single propeller is more challenging. The strong rolling moment introduced by the propeller, has an apparent impact on the trim of the vehicle.

2.3. Revised Main Rotor

The main rotor of the first HSR was related to the parameters of the NATO-GR. As Figure 1 shows, NATO-GR and HSR have identical four-bladed main rotors with identical blade planform. More precisely, both rotors feature a disc loading of *DL* = 463 N/m², a solidity of $\sigma = 0.0825$, with a hover tip speed of v_{tip} = 220.9 m/s. One conclusion from the first study was a revision of the main rotor design with a parameter setup for an unloaded rotor operated at a high advance ratio.

The lift share between main rotor and wing is of particular importance. The compound rotorcraft is a complex vehicle, featuring characteristics of fixed-wing and rotary-wing aircraft. To designate this vehicle as a rotorcraft, the main rotor has to carry more than 50% of the total lift. An estimation of the rotor's remaining share of the weight force μ_G is given by equation (3). The maximum allowable blade loading for the design speed v_h is given by $(C_T/\sigma)_{red}$. The maximum speed on the advancing rotor side at $\Psi = 90°$ is given by the critical Mach number Ma_{crit} = 0.88. The rotational speed of the main rotor will be reduced by this value. Further parameters are disc loading *DL*, rotor solidity σ, as well as air density ρ and sonic speed a.

$$\mu_G = \left(\frac{C_T}{\sigma}\right)_{red} \rho \left(Ma_{crit}\, a - v_h\right)^2 \frac{\sigma}{DL} \quad (3)$$

The equation neglects the aerodynamic downforces, especially from fuselage and stabilizers, but delivers a clear design guideline. In order to keep the tail boom as short as possible, the disc loading is increased to *DL* = 500 N/m². Higher values would not be suitable since they negatively impact the lift share and rising downwash velocity. To compensate for the higher disc loading and increase the lift share of the main rotor, the rotor solidity is increased to $\sigma = 0.12$. Consequently, the number of blades was increased from four to six. Furthermore, with the reduction of blade loading in hover, the aerodynamic capabilities for a HOGE in hot and high environments improve. Considering an army hot day with 35°C and 1829 m altitude (95°F and 6000 ft) the blade loading will increase from $C_T/\sigma = 0.077$ at ISA mean sea level to $C_T/\sigma = 0.103$. It is desirable to keep the blade loading below $C_T/\sigma = 0.11$ for helicopter main rotors since the first stall may occur at $C_T/\sigma = 0.12$. The hot and high blade loading of the original four-blade rotor is $C_T/\sigma = 0.139$. The revised HSR configuration with the six-blade main rotor is shown in Figure 2.

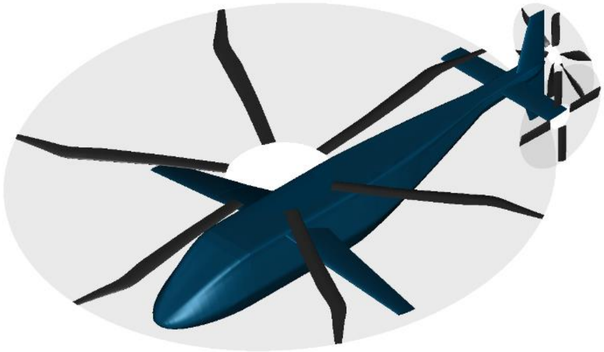

Figure 2: 3D model of the revised HSR design.

The reduced blade loading $(C_T/\sigma)_{red}$ is kept at 0.05 and the hover tip speed is v_{tip} = 220 m/s. By the new rotor and applying a different blade geometry based on the ERATO blade design [13], Ma_{crit} is increased from 0.*88* to 0.9. The blade features a first forward, then backward swept area on the outside, shown in Figure 2. Originally designed to reduce the noise caused by blade-vortex-interaction, the ERATO blade also showed performance benefits at higher flight speeds, due to the blade sweep in the area of high Mach numbers. The original blade features a linear base twist -10°/R that need to be reduced to -7°/R. A comparison of the blade twist is shown in Figure 3.

Figure 4 shows the Mach number in the rotor plane at maximum speed of 125 m/s. The influence of the relatively strong sweep on the outer blade can be identified by the kinked isolines and the lowered Mach numbers.

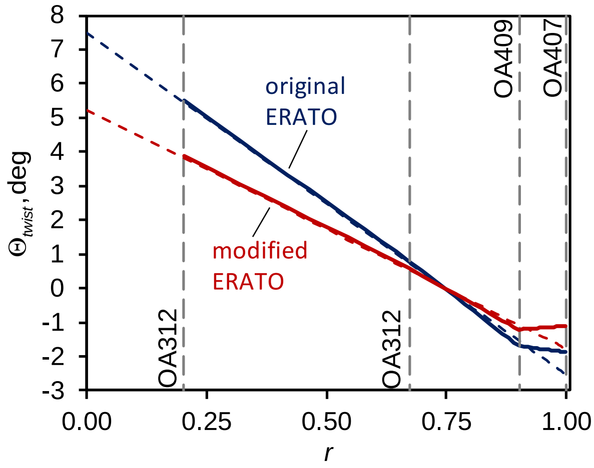

Figure 3: Comparison of the main rotor blade twist for the original ERATO blade and the modified ERATO blade of the HSR.

In Addition, Figure 5 shows the angles of attack in the same flight condition. Critical blade sections are formed by the combination of high Mach numbers and angles of attack away from 0°, which is given at Ψ = 90°.

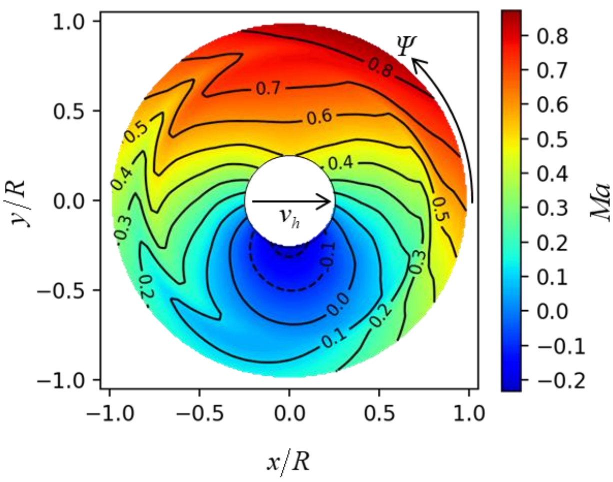

Figure 4: Mach number in the main rotor plane of the HSR at v_h = 125 m/s and μ = 0.69.

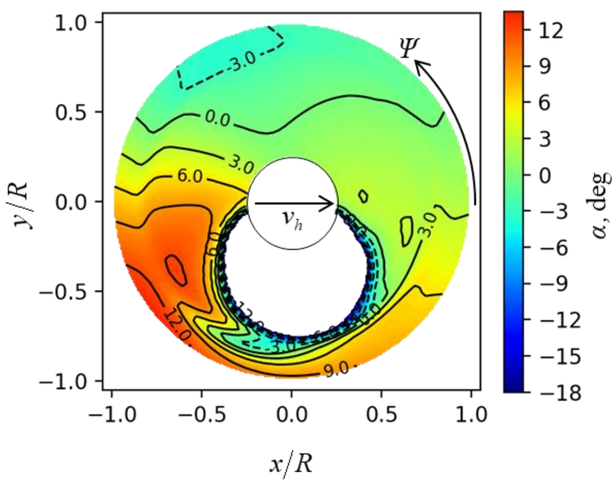

Figure 5: Angle of attack in the main rotor plane of the HSR at v_h = 125 m/s and μ = 0.69.

Figure 6 and Figure 7 show the non-dimensional contribution to the torque from the blade sections. The values are given for every element by the drag coefficient multiplied by the square of the Mach number multiplied by the non-dimensional radius. Figure 6 shows the contours of the old baseline HSR design from 2024 HSR design (see Figure 1) and values for the revised HSR can be seen in Figure 7. The area with values higher than 2.0 are significantly smaller.

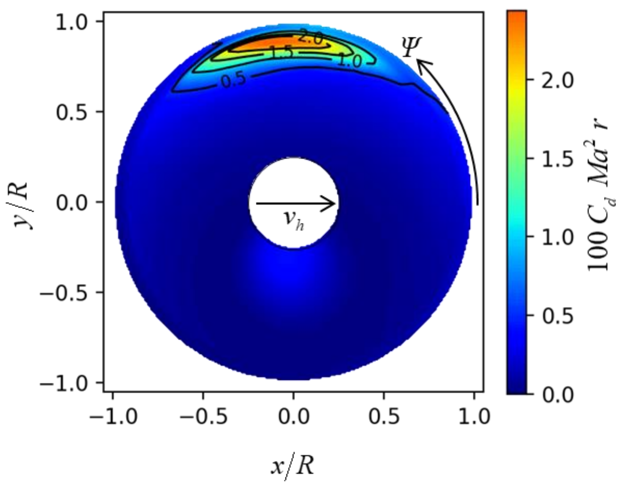

Figure 6: Non-dimensional contribution to the torque in the main rotor plane of the baseline HSR at v_h = 125 m/s, featuring the NATO-GR related main rotor with four blades at μ = 0.71.

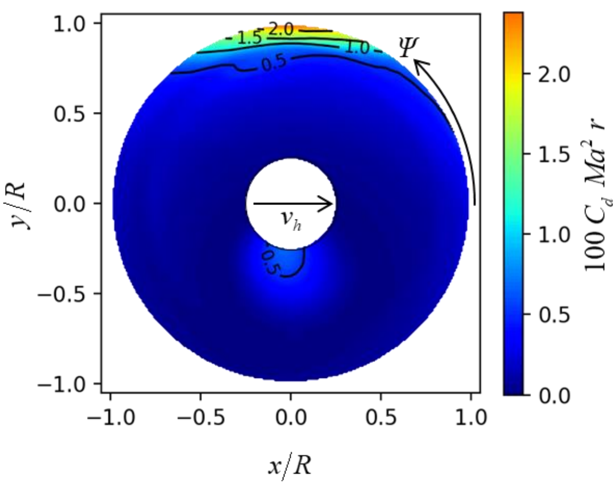

Figure 7: Non-dimensional contribution to the torque in the main rotor plane of the revised HSR at v_h = 125 m/s, featuring the new main rotor with six blades at μ = 0.69.

The choice of parameters for the rotor is apparently sensible and shows slight improvements, although the disc loading and critical Mach number have been raised. The primary objective of the new main rotor is to increase the lift share of the rotor, which is shown in Figure 8. The solid lines show the revised HSR, while the dashed lines represent the former design.

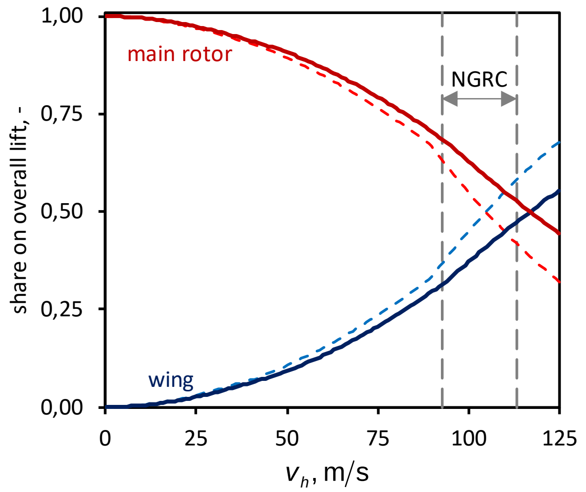

Figure 8: Wing/Rotor lift share ratio of original and revised HSR design.

The trim calculation underlined the success of the new rotor design. The point at which the lift is equally shared between the main rotor and the wing has been shifted to higher flight speeds, beyond the speed range specified for NGRC. For all design scenarios analyzed in this study, the main rotor now features more than 50% of the total lift. Furthermore, the wing size could be reduced by 30%.

2.4. Controls

The controls of the main rotor and tail rotor for the revised HSR are shown in Figure 9. For reference, the maximum flight speed of the NATO-GR (82 m/s) and HSR (125 m/s), as well as the NGRC (93 m/s – 113 m/s) interval, are marked. Longitudinal and collective main rotor controls show a constant increase in the extended flight envelope. In the design range for NGRC no difficult characteristics are visible.

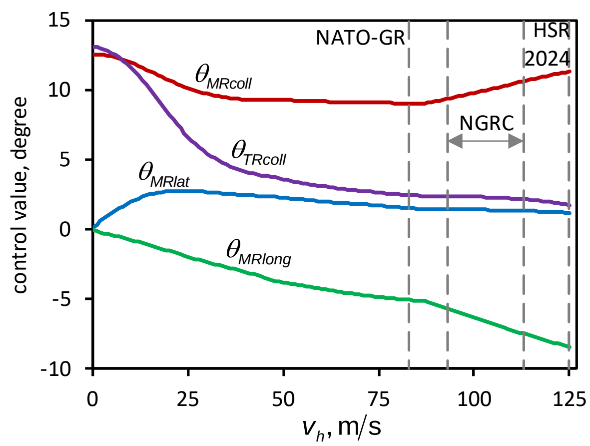

Figure 9: Main and tail rotor control angels.

The deflections of the elevator, ailerons, and flaps are shown in Figure 10.

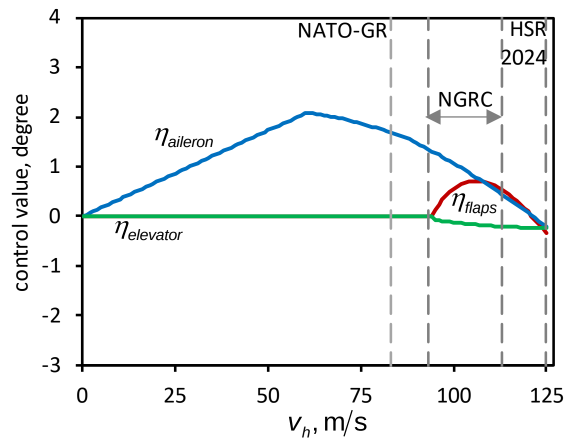

Figure 10: Deflection of the control surfaces on wings and stabilizers.

It's worth noting that ailerons and flaps are identical control surfaces with the exception, that flaps mean the symmetric deflection and ailerons the asymmetric deflection of the control surfaces on the wings. Rudder control is integrated in the flight model but not included in the trim.

The wings and stabilizers are set at an angle of incidence relative to the fuselage to achieve a streamlined configuration at high speeds with minimal required deflections of the control surfaces. A notable characteristic is observed in the fourth trim law, where the flaps exhibit highest deflections starting at 95 m/s. Between 95 m/s and 107 m/s, the lift shifted from the rotor to the wing exceeds the lift increase due to rising dynamic pressure. From 107 m/s on, the quadratic relationship between dynamic pressure and flight speed surpasses the lift shift, resulting in decreased flap deflections. Consequently, the design speed for the wing area lies between 93 m/s and 113 m/s. Given the slight flaps deflection range of -0.3° to 0.7°, the wing area is appropriately suited for the examined velocity range and requires no further modification.

2.5. Overall Characteristics and Performance

The HSR was resized for the design speed of 125 m/s and a mission radius of 201 km based on the revised design synthesis. The results are presented in Table 1, relating them with the NATO-GR. Compared to the previous study, the MTOM has decreased from 17.5 t to 15.7 t., primarily due to a new setup for estimating the drive system mass.

Table 1: Characteristics of the revised HSR with a design flight speed 125 m/s and a 201 km mission radius.

Characteristic	NATO-GR	HSR	
MTOM	9,926 kg	15,681 kg	+58.0%
BEM	6,191 kg	10,743 kg	+73.5%
Fuel mass	1,305 kg	2,505 kg	+92.0%
MCP	2,558 kW	7,080 kW	+176.8%
MR radius	8.150 m	9.896 m	+21.2%
TR radius	1.675 m	2.063 m	+23.2%
Prop. radius		2.138 m	
Wing Area		13.752 m²	

The corresponding range and endurance diagram for the revised HSR and NATO-GR is shown in Figure 11.

Despite the HSR having 92% (1200 kg) more fuel, the maximum range increases by only 9% (56 km), while the maximum endurance decreases by 13.3% (26 min).

Despite the revised HSR design, the fundamental results of the first HSR study remain valid: The HSR is an effective but inefficient rotorcraft. The need of a more detailed investigation of the design space between conventional NATO-GR and HSR with a maximum speed of 125 m/s is evident.

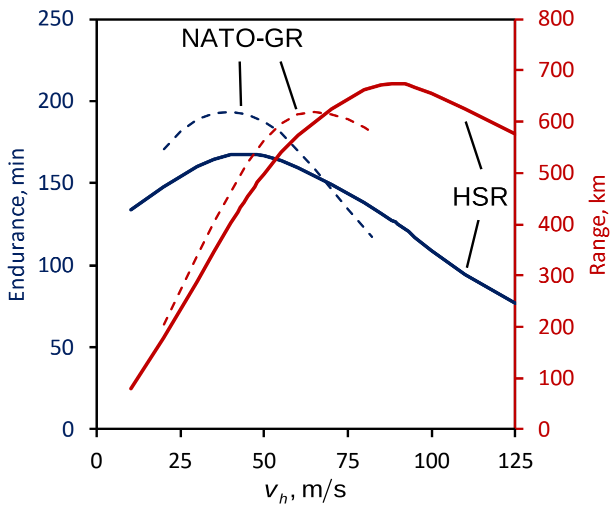

Figure 11: Range / Endurance diagram of the resized HSR configuration compared with the NATO-GR

3. DESIGN REQUIREMENTS

3.1. Performance requirements

The maximum flight speed requirement of the NGRC, ranging from 93 m/s to 113 m/s, will be examined using four evenly distributed speeds: 93 m/s, 99 m/s, 106 m/s, and 113 m/s. The installed power is determined by the trim power at these flight speeds. The relationship of the MCP and the trim power is shown in Equation (4).

$$P_{MCP} = \left(P_{vMax} \frac{1}{\eta_{mech}} + P_{sys} \right) \cdot 1.05 \quad (4)$$

Here, the required power at maximum speed P_{vMax} is adjusted by the mechanical efficiency η_{mech}, and systems power P_{sys}, and is subsequently increased by

5%. In this study the efficiency is set at η_{mech} = 0.98 and the systems power at P_{sys} = 50 kW.

3.2. Design Mission Requirement

The mission profile for an air assault is a common requirement for design studies of medium rotorcraft and is illustrated in Figure 12. It typically undergoes minor variations across different studies by NATO Applied Vehicle Technology (AVT) research groups, such as AVT-319 “High Speed Rotorcraft Analysis and Evaluation”, or AVT-378 “Progressive Rotorcraft Propulsion Alternatives”.

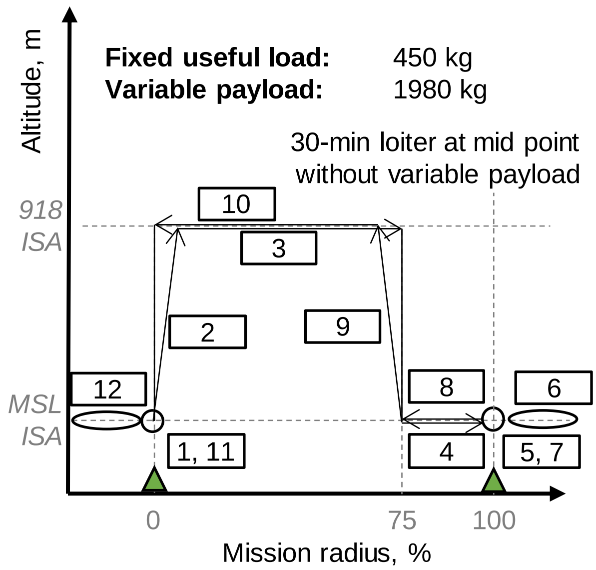

Figure 12: Design mission profile “Air Assault”.

In the current study the mission comprises 12 flight segments and starts with a 60-second HOGE at mean sea level (1) representing all start-up procedures including take-off. The next segment involves a maximum effort climb to cruise altitude (2), followed by a cruise flight at speed for best range until 75% of the mission radius is reached (3). The final 25% of the mission radius is flown at mean sea level with the configuration's maximum speed (4). Segments 2, 3, and 4 contribute to the mission radius. At the mission radius, a 60-second HOGE represents short a landing, during which 1980 kg of payload (12 to 14 troops) is dropped and then the rotorcraft takes off again (5). This is followed by a 30-minute loiter at best endurance speed (6) followed by a 60 s HOGE for picking up 1980 kg of payload before leaving the area (7). The return to base is represented by a low-level cruise at maximum speed over 25% of the mission radius (8), followed by a maximum climb to cruise altitude (9) and a best-range cruise flight (10). For landing, a 60-seconds HOGE is performed (11), followed by a 30-minute reserve at best endurance speed (12). The minimum mission radius is 200 km, close to the former study. The maximum radius shall be 400 km, and a medium scenario is included with 300 km mission radius.

3.3. Off-Design Mission Requirements

A detailed analysis of the off-design capabilities is performed through the computation of three additional mission profiles. In contrast to the balanced design mission, the off-design missions focus more specifically on best range, best endurance, and maximum speed, while still including ancillary segments such as take-off, landing, climb, reserve, and others. The first off-design mission is self-deployment, illustrated in Figure 13.

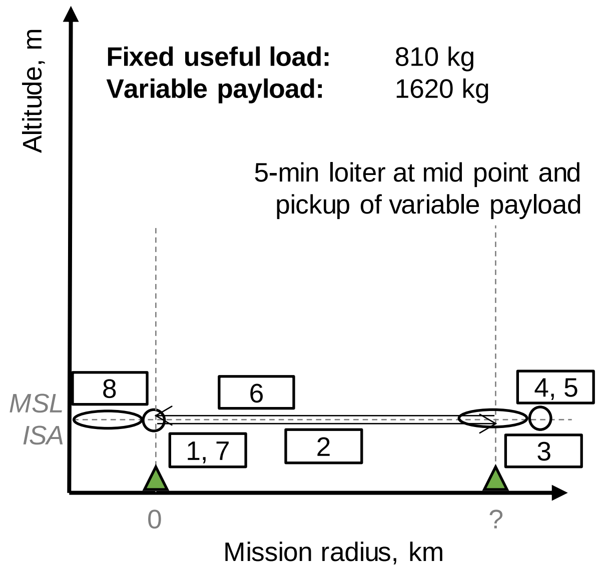

Figure 13: Mission profile for self-deployment.

The mission emphasizes the speed for best range. The fixed useful load comprises the crew, additional load handling systems for external loads, and the structure of external fuel tanks. The initial fuel mass includes the design fuel mass and additional 1100 kg fuel, which are stored in the external tanks. The cruise segment 3 is flown at an altitude of 918 m at the speed for best range. The length of the cruise segment is computed with respect to the available fuel. The reserve is flown with best endurance for 30 minutes.

The second off-design mission focuses on maximum speed, specifically for medical evacuation (medevac), as seen in Figure 14. It begins with take-off (1), followed by a maximum speed cruise to the mission radius (2), a 5-minute loiter (3), landing (4). On the ground, the variable payload is picked up, followed by take-off (5), and return to base with maximum speed (6), landing (7) and a reserve segment (8). The possible mission radius is calculated based on the available fuel.

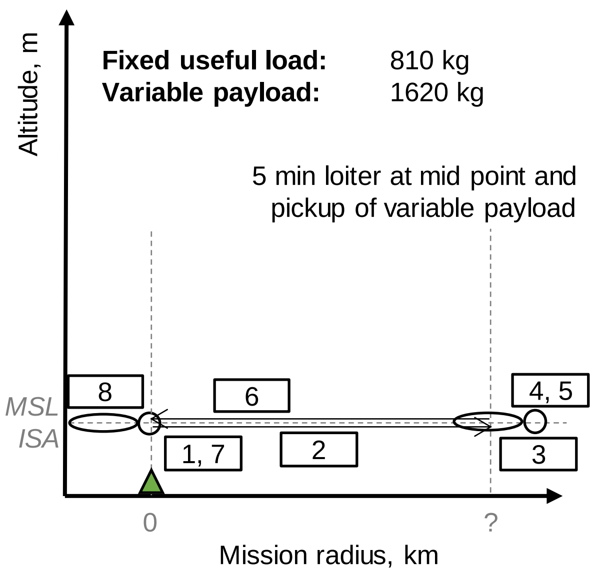

Figure 14: Mission profile for medical-evacuation.

The third mission, focusing on endurance, pertains to a blue water operation. Figure 15 shows a potential mission profile, highlighting a flight mission over open water with take-off and landing on a ship.

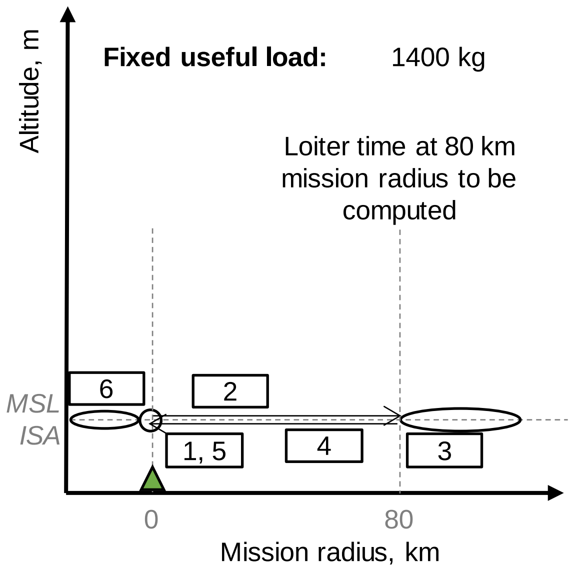

Figure 15: Mission profile for blue water operation.

The focus is on the rotorcraft's surveillance/endurance capabilities in an area of interest. Here, the mission starts with take-off (1), followed by a cruise at best-range speed to 80 km (2) and a loiter at best-endurance speed (3) in the surveillance area. Loiter time is computed from the available fuel. Finally, the rotorcraft returns to the ship with a best range cruise (4), lands (5), and has a 30-minutes reserve (6). The payload remains constant at 1400 kg.

4. EVALUATION

4.1. Characteristics

Four flight speeds and three missions result in a matrix of 12 different versions of the compound rotorcraft. Figure 16 shows the design space with the NATO-GR at 82 m/s and the HSR at 125 m/s flight speed as references. Here, the iso-lines for mission radius are blue, and iso-lines for design velocities are red.

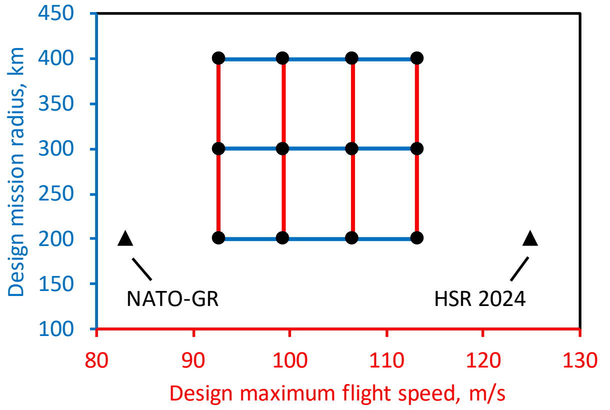

Figure 16: Design space in relation to NATO-GR and HSR.

The design and sizing tasks were solved by IRIS. The MCP plotted over MTOM is shown in Figure 17. The MTOM ranges from 12.3 t < m_{MTOM} < 16.5 t. The limit of 15 t, which is a consideration for most ship decks, is marked by the dashed grey line. The NATO-GR and the HSR for 125 m/s, both with a 201 km design mission radius, are also shown. This indicates, how far these two configurations are outside the design space.

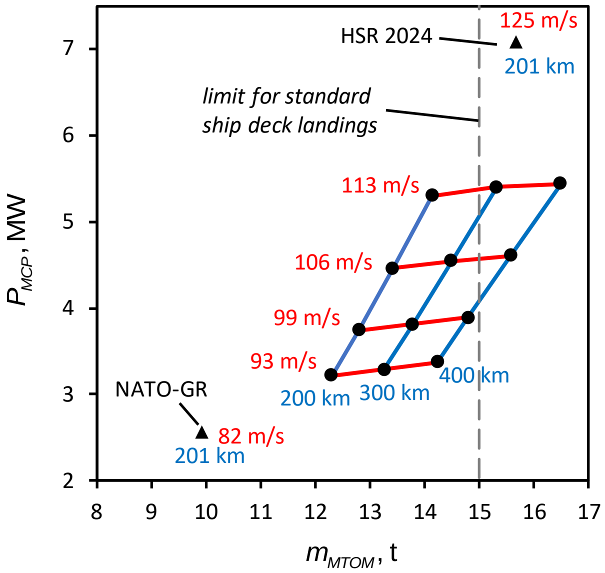

Figure 17: Maximum take-off mass versus maximum continuous power for design space.

The installed power ratio is given by Equation (5). It is sensible to assess or even size the power with respect to the dimensions of the vehicle. The relationship to the ideal power is calculated considering the maximum take-off mass m_{MTOM}, gravitational acceleration g, density of air ρ, and the main rotor radius R. With the P_{inst}/P_{ideal}, it is possible to size, or to evaluate the power ratings.

$$\frac{P_{inst}}{P_{ideal}} = P_{inst}\left(\sqrt{\frac{(m_{MTOM}\,g)^3}{2\,\rho\,\pi\,R^2}}\right)^{-1} \tag{5}$$

As mentioned in section 3.1, the installed power is sized by the required power for the design speed (see Equation (4)). In contrast, Equation (5) is used to evaluate the installed power for vertical flight. Typical values for P_{inst}/P_{ideal} for two engine rotorcraft should be around 2.5 [14]. The values for the 12 design configurations are shown in Table 2. Here, the values for the design speed 93 m/s indicate a potentially too low installed power with respect to the weight force. For most high-speed configurations the installed power, that is required for fast flight, exceeds the required power for vertical flight.

Therefore, more specific requirements for hot and high flight conditions, vertical climb, as well as one engine inoperative (OEI) are necessary. Apparently, the design speed of 93 m/s highlight the area of transition from a conventional helicopter to a compound rotorcraft.

Table 2: Installed power ratio within the design space.

v_{design}	*Design mission radius*		
m/s	200 km	300 km	400 km
113	3.715	3.493	3.268
106	3.294	3.106	2.930
99	2.897	2.742	2.602
93	2.595	2.455	2.350

The influence of the flight speed becomes apparent. For instance, the sizing with the combination of 113 m/s and 200 km shows a MTOM of 14.1 t. In contrast, the combination of 93 m/s speed and 300 km mission radius results in a MTOM of 13.8 t.

Figure 18 shows the fuel mass over the basic empty mass (BEM). An increase of installed power increases the fuel consumption. Every increase of the fuel mass results in an increase of the BEM, since the fuel must be transported. With increasing maximum flight speed, the basic empty mass rises stronger than the fuel mass. The main reason is the upscaling of the drive system, which also depends on the installed power. Consequently, the variation in speed has the highest impact on the BEM. In contrast, the allocation of the blue iso-lines points out the high dependency of the flight range on the fuel mass, with a weaker influence on the BEM.

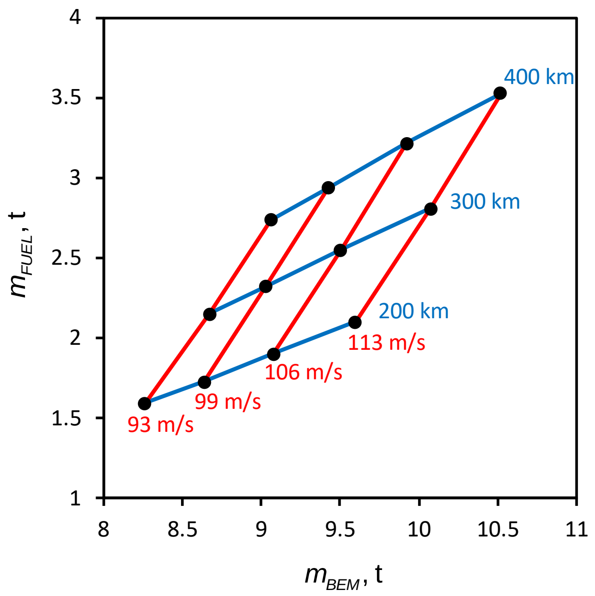

Figure 18: Basic empty mass versus fuel mass for the design space.

The configuration with 93 m/s and 300 km features a design fuel mass of 2.15 t compared to 113 m/s and 200 km, which requires a fuel mass of 2.1 t. In contrast to nearly identical fuel masses, the BEM of the faster configuration is 10.7 % (926 kg) higher.

It's worthy to note that the configurations on the red iso-line for 93 m/s could be replaced by a conventional configuration featuring a main rotor and anti-torque only. Without compound items like wings and propellers, the BEM would decrease. The flight speed of 93 m/s (180 kn) is ambitious but considered possible for a conventional helicopter.

4.2. Flight Performance

This subsection focuses on performance indicators such as maximum range and endurance, and their relationship to the required fuel mass. Maximum range and maximum endurance are calculated using the respective flight speeds of best range and best endurance for each configuration. The fuel mass over the maximum range is shown in Figure 19.

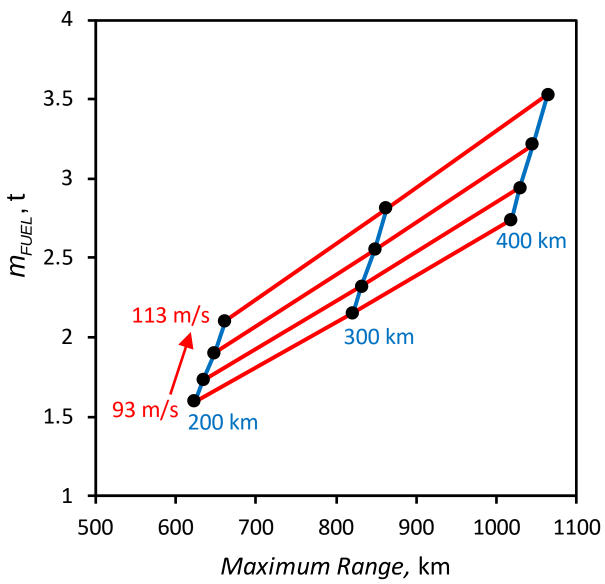

Figure 19: Maximum range versus fuel mass.

In the previous example (93 m/s with 300 km and 113 m/s with 200 km), nearly identical fuel masses were observed, either due to higher speed or higher range requirements. The *slow* configuration has a best range speed of v_{BR} = 76 m/s with a maximum range of 821 km. The best range speed of the *fast* is v_{BR} = 79 m/s, with a maximum range of 661 km. It is apparent how opposing maximum speed and range are and how challenging it is to combine them.

Furthermore, for every blue iso-line, the range increases with increasing maximum speed, but only by a small amount compared to the fuel mass. For instance, comparing the configurations of 93 m/s and 113 m/s for the 300 km line, shows a +5% (41.5 km) increase in range with an increase in fuel mass of about +30% (658 kg).

The fuel mass as a function of the maximum endurance is shown in Figure 20. Here, the endurance even decreases along the blue isolines with increasing maximum speed. For example, along the iso-line of 300 km, the possible endurance decreases by -6.5%

(15.4 min) considering a +30% (658 kg) increase in fuel mass.

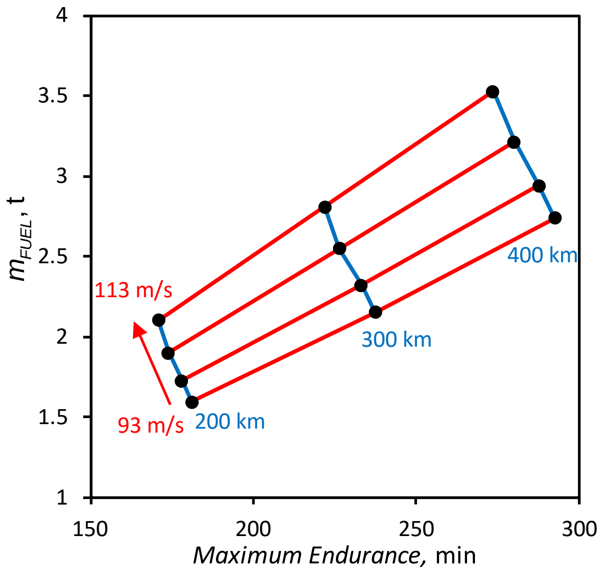

Figure 20: Maximum endurance versus fuel mass.

The specific range and endurance are given with Figure 21 by dividing the maximum range and endurance by the design fuel mass. Here, an increase in efficiency of range as well as in endurance can be seen with decreasing maximum flight speed. The distinction is made by the four design speeds, resulting in four groups comprising the three mission ranges.

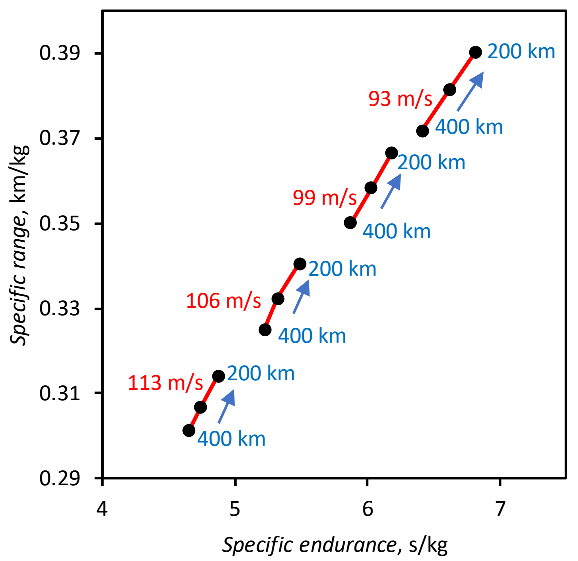

Figure 21: Specific range versus specific endurance.

4.3. Off-Design Mission Performance

The values for specific range and endurance are averaged values. A further analysis, in addition to these, involves considering a full mission profile. This includes parasitic flight segments such as take-off, landing, loiter, and others. By examining a self-deployment mission (Figure 13) and a blue water mission (Figure 15), the focus is on the relationship between best range and best endurance. Figure 22 shows the resulting endurance in a blue water operation over the self-deployment distance. The diagram clearly groups the design space according to the three distance requirements. Regarding the influence of the required maximum speed, there is no contact or even overlap between these groups. By focusing on effective numbers, Figure 22 shows the reverse characteristics of Figure 21.

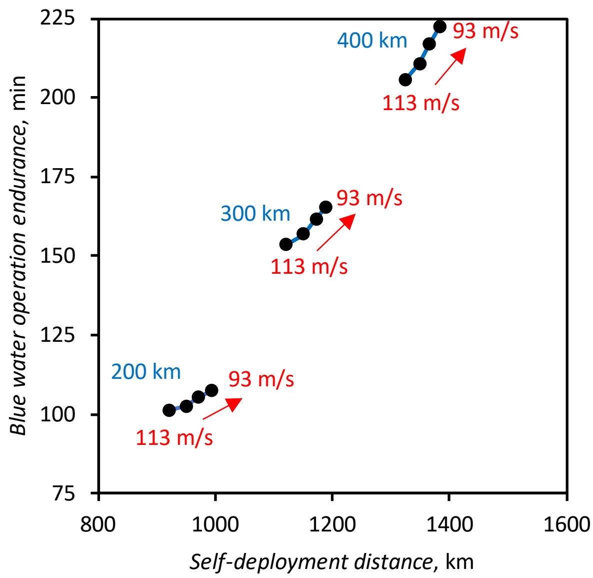

Figure 22: Self-deployment distance versus endurance for blue water operation.

Substituting the blue water mission with the medevac mission (Figure 14), the second criterion is now the possible mission radius applying maximum flight speed and returning with the variable payload mass from the midpoint. The results are plotted in Figure 23. Like Figure 22, the presentation of two effective flight performance characteristics highlights the primary impact of the range requirement.

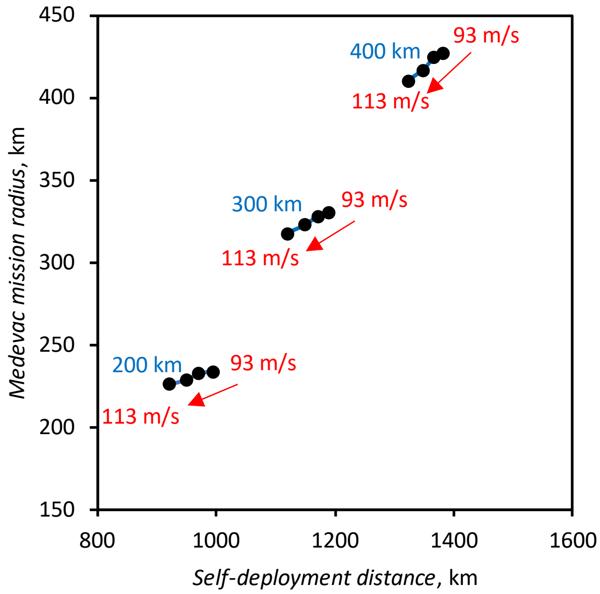

Figure 23: Self-deployment distance versus medevac mission radius.

Figure 24 shows the fuel mass over the self-deployment distance. Here, the fuel mass comprises the design fuel mass plus the 1100 kg inside an extra fuel tank. The grouping according to the range requirement is not as clear as in Figure 22 and Figure 23. It should be noted that the blue isolines are contrary to those in Figure 19, as extra fuel and a full mission are considered. With an increasing speed requirement, the self-deployment distance decreases.

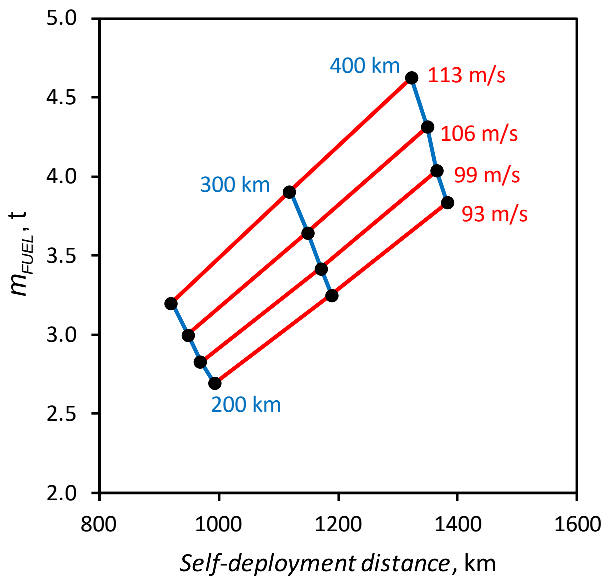

Figure 24: Self-deployment distance versus mission fuel mass (design fuel mass plus 1100 kg extra fuel).

The fuel mass over the radius of the medevac mission is shown in Figure 25. In contrast to Figure 24, the diagram considers only the design duel mass. What stands out are the different design fuel masses with respect to the speed requirements. The change in the medevac mission radius with respect to the speed requirements, considering a constant range requirement, are minimal.

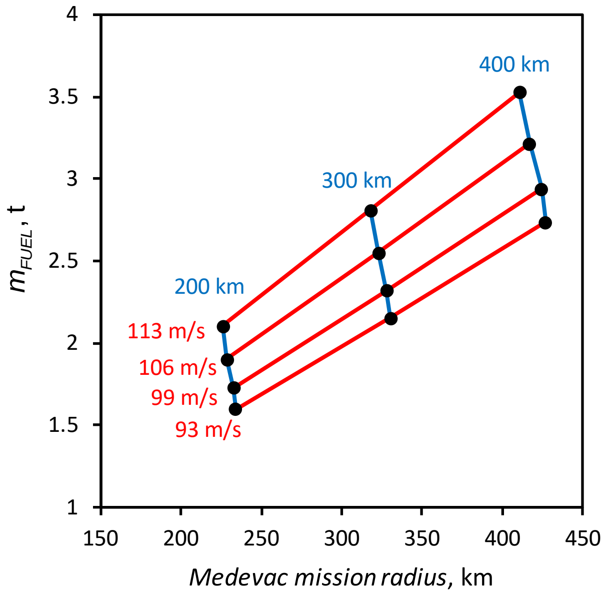

Figure 25: Medevac mission radius versus fuel mass.

In addition to Figure 25, the basic empty mass over the medevac mission radius is plotted in Figure 26.

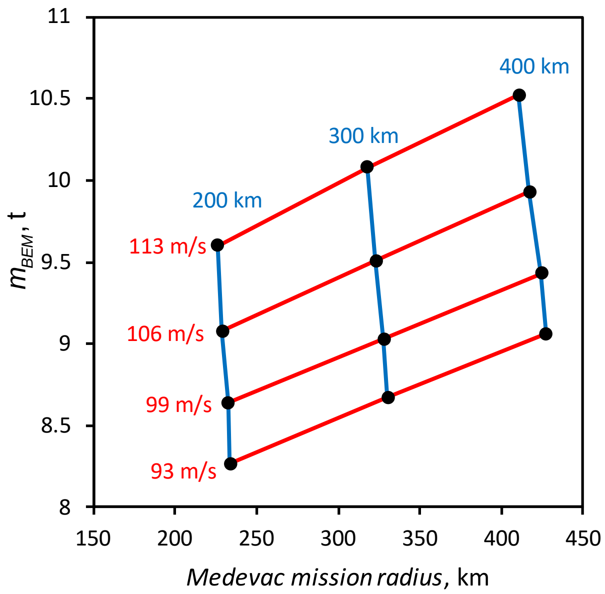

Figure 26: Medevac mission radius versus basic empty mass.

Compared to the flight distance, the design speed has a crucial impact on the basic empty mass. By comparing Figure 25 and Figure 26 in combination with Figure 18, it becomes clear how strong the dependency of the speed requirement on the BEM is. With increasing design speed, the required installed power rises, so does the mass of the drive system, including the gearbox and power transfer. With increased power of the engine, more fuel is also burned during conventional flight speeds. The increased fuel mass must be transported inside the vehicle. Therefore, the speed requirement has a very strong impact on the BEM.

5. CONCLUSIONS

This paper highlighted the first results of the second HSR study in the support campaign for the Army Concepts and Capabilities Development Centre. The key question was the influence of variable maximum speeds and mission ranges on compound rotorcraft. By investigating the NGRC speed interval ranging from 93 m/s to 113 m/s (180 kn to 220 kn), several findings were derived:

- The revised HSR configuration showed a reduction of the MTOM of 10%, enabling the main rotor to generate more lift over the flight envelope, but the fundamental problem of inefficiency in the conventional flight envelope remains.
- The impact of the range requirement in the design mission has the most significant influence on the performance characteristics of the design configuration, considering the full range of possible design speeds.
- The speed requirement showed a high impact on the installed power and furthermore the basic empty mass and the maximum take-off mass.
- The lower flight speeds of 93 m/s (180 kn) can also be achieved by a highly performant, but still conventional helicopter. The absence of wings and propellers will reduce the basic empty mass but limit the flight speed absolutely.
- For the DLR design activities, this was the first investigation applying a sweep of the requirement parameters. The buildup of IRIS, especially considering its modular structure and universal data model, proved to be highly practical. Here, the use of CPACS for input and output resulted in noticeable time savings.

The findings presented in this paper result in several options on how to progress. The next study will focus on the critical distinction between a conventional and a compound rotorcraft. The compound is the enabler for a higher flight speed. The choice for a conventional helicopter focuses the design on a more efficient vehicle. A study will be conducted with both configurations including a variation of flight speed for the HSR. In order to narrow the design space, a design mission with sensible range and performance requirements is essential.

Author contact:

Peter Weiand peter.weiand@dlr.de

Kagan Atci kagan.atci@dlr.de

Dominik Schwinn dominik.schwinn@dlr.de

REFERENCES

1. Weiand, P., Atci, K., Schneider, O., Graaf, S. de, Herzig, J., Winkler, L., Cornelje, S., Schwinn, D., Inac, H., Reimer, F., Lindlar, M., Mainz, H., Dias Fernandes, C., Becker, R., "Development of a New Fleet Concept for HEMS Operations," Vertical Flight Society's 81st Annual Forum & Technology Display, Virginia Beach, VA, USA, 20-22 May, 2025

2. Weiand, P., Atci, K., Schwinn, D., "High-Speed Compound Rotorcraft Performance and Design," Vertical Flight Society's 80th Annual

Forum & Technology Display, Montréal, Canada, 7-9 May, 2024

3. Silva, C., Yeo, H., Johnson, W., "Design of a Slowed-Rotor Compound Helicopter for Future Joint Service Missions," American Helicopter Society Aeromechanics Specialist's Conference, San Francisco, CA, USA, 20 January 2010

4. Eglin, P., Embacher, M., Desvigne, D., Roca-Leon, Enric, "Airbus RACER High Speed Demonstrator Flight Tests," Vertical Flight Society's 81st Annual Forum & Technology Display, Virginia Beach, VA, USA, 20-22 May, 2025

5. Hilbert, K. B., "A Mathematical Model of the UH-60 Helicopter. NASA TM 85890 and USAAVSCOM TM-84-A-2. Ames Research Center, Moffett Field, CA, USA (1984)

6. Yeo, H., Bousman, W. G., Johnson, W., "Performance Analysis of a Utility Helicopter with Standard and Advanced Rotors," American Helicopter Society Aerodynamics, Acoustics, and Test and Evaluation Technical Specialist Meeting, San Francisco, CA, USA, 23-25 January, 2004

7. Böhnke, D., Litz, M., Rudolph, S., "Evaluation of Modeling Languages for Preliminary Airplane Design in Multidisciplinary Design Environments," Deutscher Luft- und Raumfahrtkongress 2010, Hamburg, Germany, 31 August - 03 September, 2010

8. Nagel, B., Böhnke, D., Gollnick, V., Schmollgruber, P., Rizzi, A., La Rocca, G., Alonso, J. J., "Communication in Aircraft Design: Can we establish a common language?," 28th International Congress of the Aeronautical Science, Brisbane, Australia, 23 - 28 September, 2012

9. Jepsen, J., Ciampa, P. D., Nagel, B., "Design of a Common Library to Simplify the Implementation of Aircraft Studies in CPACS," Deutscher Luft- und Raumfahrtkongress 2015, Rostock, Germany, 22-24 September, 2015

10. Seider, D., Fischer, P. M., Litz, M., Schreiber, A., Gerndt, A., "Open Source Software Framework for Applications in Aeronautics and Space," IEEE Aerospace Conference, Big Sky, MT, USA, 3–10 March, 2012

11. Benoit, B., Dequin, A.-M., Kampa, K., Grünhagen, W. von, Basset, P.-M., Gimonet, B., "HOST, a General Helicopter Simulation Tool for Germany and France," American Helicopter Society 56th Annual Forum, Virginia Beach, VA, USA, 2-4 May, 2000

12. Hofmann, J., Weiss, F., Mindt, M., "A New Approach to Comprehensive Rotorcraft Aeromechanics Simulation," Vertical Flight Society's 77th Annual Forum & Technology Display, Virtual, 10-14 May, 2021

13. van der Wall, B. G., Kessler, C., Delrieux, Y., Beaumier, P., Gervais, M., Hirsch, J.-F., Pengel, K., Crozier, P., "From Aeroacoustics Basic Research to a Modern Low-Noise Rotor Blad." Journal of the American Helicopter Society, Vol. 62, (4), pp. 1–16. https://doi.org/10.4050/JAHS.62.042001

14. Weiand, P., Schwinn, D., Schmid, M., Buchwald, M., "A multidisciplinary process for integrated rotorcraft design." CEAS Aeronautical Journal, Vol. 11, (1), pp. 145–160. https://doi.org/10.1007/s13272-019-00408-y